The Astrophysical Journal Letters, 946:L17 (8pp), 2023 March 20 https://doi.org/10.3847/2041-8213/acc0f1

Statistical Study of Ejections in Coronal Hole Regions As Possible Sources of Solar Wind Switchbacks and Small-scale Magnetic Flux Ropes

Nengyi Huang[1,2], Sophia D'Anna[1], and Haimin Wang[1,2]
[1] Institute for Space Weather Sciences, New Jersey Institute of Technology, 323 Martin Luther King Blvd., Newark, NJ 07102-1982, USA; nh72@njit.edu
[2] Big Bear Solar Observatory, New Jersey Institute of Technology, 40386 North Shore Lane, Big Bear City, CA 92314-9672, USA
Received 2022 December 12; revised 2023 March 2; accepted 2023 March 2; published 2023 March 27

Abstract

The omnipresence of transient fluctuations in the solar wind, such as switchbacks (SBs) and small-scale magnetic flux ropes (SMFRs), have been well observed by the in situ observation of Parker Solar Probe (PSP), yet their sources are not clear. Possible candidates fall into two categories: solar origin and in situ generation in the solar wind. Among the solar-origin scenarios, the small-scale activities (such as ejections and eruptions) in coronal hole (CH) regions, where solar wind originates, are suggested as candidates. Using full-disk extreme ultraviolet images from Atmospheric Imaging Assembly on board the Solar Dynamic Observatory, we identify small-scale ejections in CH regions during PSP Encounters 5, 7, and 8, and study their statistical properties. These ejections belong to two categories: standard jets and blowout jets. With 27,832 ejections identified in 24 days (about 2/3 of them are blowout jets), we updated the expected frequency for PSP to detect their counterparts in the heliospace. The ejections we identified are comparable to the frequency of PSP-detected SMFRs, but they are insufficient to serve as the only producer of SBs or SB patches. Certain smaller events missed by this study, such as jetlets, may fill the gap.

Unified Astronomy Thesaurus concepts: Solar coronal holes (1484); Solar coronal transients (312); Jets (870)

Supporting material: animation

1. Introduction

Switchbacks (SBs) in the solar wind were discovered using Ulysses data decades ago (Forsyth et al. 1996; Balogh et al. 1999; Yamauchi et al. 2002. Recently, Parker Solar Probe (PSP; Fox et al. 2015) found that SBs frequently occur in the heliosphere, as it cruises from earth to the solar corona. The SBs are observed to be highly Alfvénic, with velocity spikes and rotation of radial magnetic field using the first-sight in situ measurement from PSP (Bale et al. 2019; Kasper et al. 2019). The formation mechanism of SBs remains a matter of debate. A number of models have been developed to explore the origin of SBs and they can be categorized into two kinds: SBs are either stimulated remotely by small transients from the solar surface or locally by fluctuation in the heliosphere (e.g., Squire et al. 2020). Those originating from the solar surface considered mechanisms such as that the interchange reconnection between closed and open magnetic field may form S-shaped folds in the magnetic field, which then propagate outwards (Yamauchi 2004; Fisk & Kasper 2020; Tenerani et al. 2020). They can also produce magnetic flux ropes that can be pushed by slow solar wind and generate the detected magnetic reversal (Drake et al. 2021; Agapitov et al. 2022), or the motion of footpoints near coronal hole (CH) boundaries, which can make the magnetic field get sheared by fast and slow solar wind through Kelvin–Helmholtz (KH) instability (Schwadron & McComas 2021).

On the other hand, many statistical studies have been performed using different definitions and criteria, and have successfully found that properties such as duration, size, orientation, and Alfvénicity vary among SBs (Bourouaine et al. 2020; Fargette et al. 2021; Laker et al. 2021; Fargette et al. 2022; Pecora et al. 2022). One nature of SBs is that they tend to appear in "patches" (Bale et al. 2019; de Wit et al. 2020). Fargette et al. (2021) studied the footpoints where PSP was connected to the solar surface as well as the timescale of SBs to find that the patches of SBs are related to the connected supergranulation scale. This provides observational support that disturbances in the solar atmosphere could be the original sources of SBs.

Some widely discussed candidates of the solar transient event to drive a perturbation in the solar wind includes the coronal jets (hereafter called jets), and minifilament (MF) eruptions, which may not be independent to each other. It is proposed that some jets are able to produce the so-called "narrow CMEs" that are observable in coronagraphs (Wang et al. 1998; Moore et al. 2015; Sterling et al. 2016) and may travel into the heliosphere. More recently, Telloni et al. (2022) observed and modeled the formation process of an S-shape structure in the solar corona and suggested interchange reconnection as the mechanism of SB generation, which is also one widely accepted trigger of jets. The jets were classically proposed to fit the flux-emergence mechanism where interchange reconnection happens between the emerging bipole and ambient open field (Shibata et al. 1992; Yokoyama & Shibata 1995), while a concept called "blowout" jet was established (Moore et al. 2010) to explain the jets associated with MF eruptions as a miniature version of coronal mass ejections, just like the nanoflares to the flares (Sterling et al. 2015). More updated observations suggested that (1) the observed occurrence rate of jets may have been limited by instruments (Hou et al. 2021), and (2) many or most of jets were associated with eruptive minifilaments (EMFs; Sterling et al. 2022). In the numerical model, Wyper et al. (2017, 2018)

Table 1
The Selected Ranges of Dates in This Study

Encounter	Selected Dates	Perihelion Date	Quasi-corotation Date
4	2020-01-23–2020-02-01	2020-01-29	N/A
5	2020-06-09–2020-06-13	2020-06-07	2020-06-10
8	2021-04-29–2021-05-07	2021-04-29	N/A

depicted the EMF-associated jets as a "breakout" model, which emphasized the role of magnetic reconnection. Sterling & Moore (2020) examined and supported the possibility that EMF associated with jets can be the driver of SBs.

From decades of observations and modeling, the omnipresence of magnetic flux ropes (MFRs) in interplanetary space (e.g., Moldwin et al. 2000; Zheng & Hu 2018; Chen et al. 2019, 2020) and the ubiquitous of their eruptions in the form of minifilaments (MF; e.g., Yang & Zhang 2018) are well known. MFRs are generally defined as a bundle of magnetic field lines that are twisted about each other and wrapped around a common axis. These current-carrying magnetic field systems are crucially important, as they may exhibit eruptive activities while subject to different modes of instabilities and forces (Myers et al. 2017). On the large scale, significant attention has been drawn to the structure and evolution of solar magnetic flux ropes, as they are believed to constitute the key component of coronal mass ejections (CMEs), a major form of solar eruptions that can have a direct impact on space weather (Chen 2017; Cheng et al. 2017). The large-scale MFRs are often in the form of filaments in the solar surface and detected in the interplanetary magnetic clouds corresponding to the CMEs (Burlaga et al. 1982), which may cause geomagnetic disturbances when interacting with Earth's magnetic field.

Equally interesting and important are small-scale MFRs (SMFRs), in the form of minifilaments (MFs) and their eruptions (Wang et al. 2000; Sterling et al. 2015). In these eruptive events, small regions of the closed magnetic field, which confine a volume of cool plasma are destabilized by the evolution of the underlying magnetic field. These structures or flux ropes can then be explosively ejected into the corona, much like larger filament eruptions. As they are numerous and ubiquitous, their effects in the corona and solar wind may be significant. Using BBSO full-disk Hα data, Wang et al. (2000) found that, on average, MFs have a length of 20 Mm, an ejection speed of 13 km s^{-1}, a mean lifetime of 1 hr, and a total mass and kinetic energy of 10^{13} g and 10^{25} ergs, respectively. MF eruptions may be the underlying cause of coronal jets and macrospicules (Sterling & Moore 2020; Baikie et al. 2022; Sterling et al. 2022). In events where an MF is visible, cool plasma (10^4 K) lying along the magnetic polarity inversion line (PIL) between the central minority polarity and the surrounding majority polarity indicates the presence of a filament channel, observed using Atmospheric Imaging Assembly (AIA; Lemen et al. 2012) data of the Solar Dynamics Observatory (SDO; Pesnell et al. 2012). Even in the absence of filament plasma, the existence of a filament channel can be deduced from the appearance of a posteruption flare arcade straddling the PIL.

The twisted SMFRs carried away with jets into the solar wind would likely produce transients throughout, which are clearly identified by in situ observations of PSP (Chen et al. 2021; Chen & Hu 2022). The authors found that their time duration and scale sizes range from 10 s to about 1 hr, and from a few hundred kilometers to 0.001 au. Furthermore, they found evidence that interchange reconnection is a possible mechanism for generating flux rope–like structures near the Sun, detected by PSP in the solar wind. However, it is still debated if these SMFRs are associated with solar sources or if they are generated locally in solar wind (Feng et al. 2008; Zheng & Hu 2018; Chen & Hu 2022). The number of SMFRs detected by PSP can be as high as 100 per day. The daily occurrence rate of larger coronal jets on the entire solar disk, as reviewed by Raouafi et al. (2016), is in the same order of magnitude. The observed coronal jets are not sufficient to account for the occurrence rate of PSP SMFRs, as PSP only detects a small fraction of events from the Sun during its passages around the Sun. Therefore, we must look into other smaller-scale eruptions/ejections as possible sources of SMFRs as well as SBs in the solar wind.

To study these small ejections and their potential to be the source of energy and perturbation that generates these small-scale events, their occurrence distribution becomes important. Savcheva et al. (2007) studied X-ray jets in the polar CH region and found their occurrence rate as 60 day^{-1} with lifetimes of $\tilde{1}$0 minutes. Based on the previously found statistics of jets, Roberts et al. (2018) estimated that PSP should encounter about one jet per 50 days. This is significantly insufficient. On the other hand, Kim et al. (2007) validated that the observations of jets on extreme ultraviolet (EUV) have similar observable properties to X-ray observations. A number of studies have observed jets on EUV data with higher image quality and reported the dynamics of jets on the small scale (Liu et al. 2011; Mandal et al. 2022). Therefore, we emphasize the importance of the statistical study of the occurrence and distribution of jets using the EUV observation. In this study, the full-disk observations from the AIA are used to identify the coronal jets in CHs. They are then grouped as either standard jets or eruptive events, and their occurrence rate, lifetime, and base size are surveyed. The statistical properties will be compared with those of SMFRs and SBs observed in the solar wind by PSP.

2. Data

We mainly use SDO/AIA data to analyze the properties of solar ejections/eruptions. In order to statistically compare the occurrence of solar events and SBs/SMFRs, we selected the data during the PSP encounters when PSP's distance to the Sun was within 0.25 au. Encounter 4, 5, and 8 (denoted as E4, E5, and E8 hereafter) were selected because during perihelia 4 and 8 the predicted PSP footpoint was on the solar disk, and during E5 the Earth's (and SDO's) sight can observe the "quasi-corotation" period when PSP footpoint corotates with the Sun. The selected dates of our analyses are listed in Table 1. AIA provides EUV images with a cadence of 12 s. To reduce the data volume without sacrificing the accuracy of event identification, we select images to have an effective cadence of 48 s.

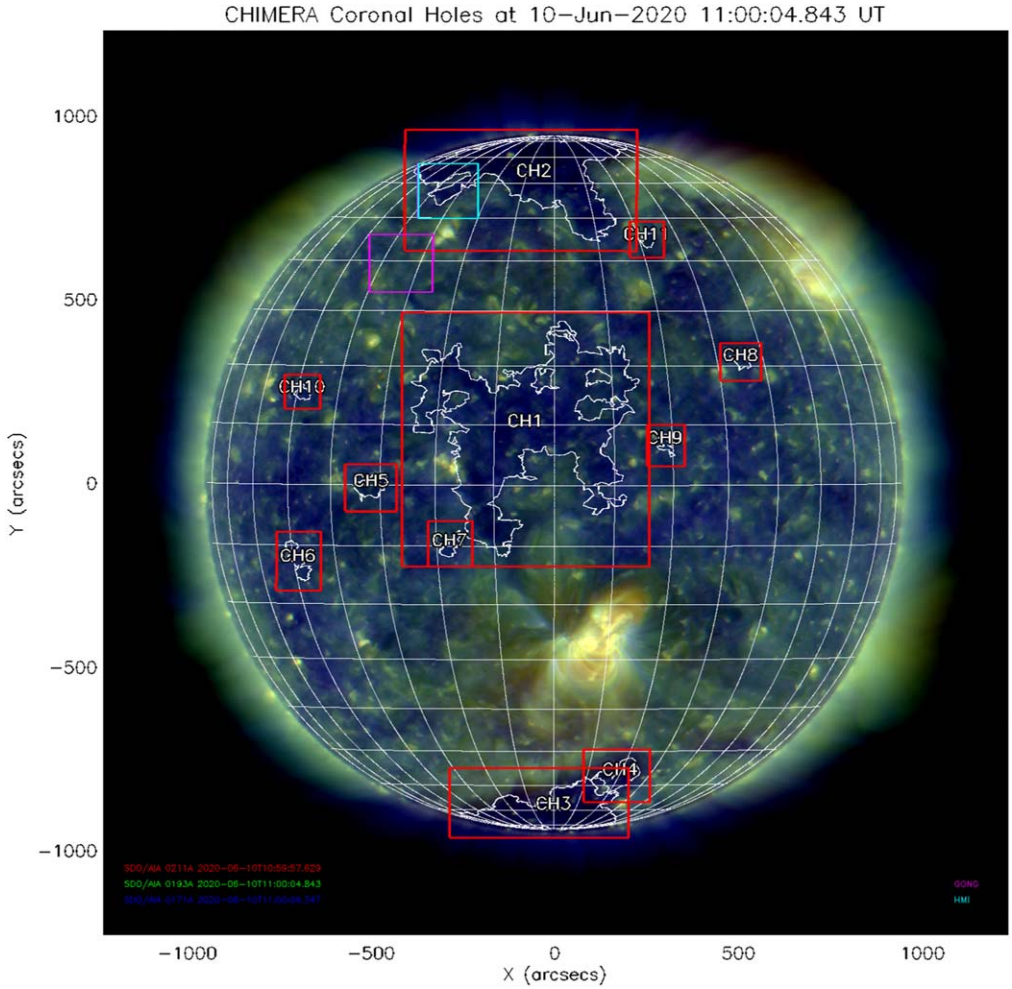

Figure 1. An example of CHs detected using CHIMERA algorithm. The background is the blended images of AIA 171, 193 and 211 Å. The white contours are the boundaries of CHs calculated hourly and combined for 4 hr, and the red solid line boxes mark the cut areas where ejections are identified. The pink and cyan rectangles are indicating the location of PSP source regions provided by the modeling team, using GONG and HMI magnetogram, respectively.

2.1. Coronal Hole Area Identification

CHs are regions in the solar corona where the magnetic fields are open and connect to the heliosphere (see Figure 1 as an example) allowing the plasma material to escape from the Sun. CHs and CH adjacent areas are generally believed to be the source regions of the fast and slow solar wind, respectively (Krieger et al. 1973; Zirker 1977). To study the source of small transients in the solar wind, we focus on the small-scale transients in the CH regions. CHs are normally observed as darker areas in EUV images of the corona. To define the CH regions, an automated CH identification algorithm, coronal hole identification via a multithermal emission recognition algorithm (CHIMERA, Garton et al. 2018), is used to map the boundaries of CHs. The emission intensity of three EUV wavelengths (171, 193, and 211 Å) are involved in the calculation of CH regions with lower temperatures, while SDO Helioseismic and Magnetic Imager (HMI) magnetograms are used to assure each region has a unipolar nature and does not have a strong line-of-sight magnetic field. The CH identifications are processed for each hour on our selected dates. To eliminate the discontinuity of CH identification that comes from the automated algorithm, we combined the hourly calculated CH for every 4 hr. Figure 1 shows an example of the CHIMERA calculated intensity image overplotted by the identified CH boundaries (white lines). For each identified CH, a rectangle area including the CH and its adjacent quiet Sun area is cut as our region of interest (denoted by the red rectangles in Figure 1), in which the ejections are to be identified. To ensure the adjacent area is included, we extended the boundaries by 25″. In addition, the pink and cyan rectangles are showing the regions covering PSP footpoints during the corresponding 4 hr, whose boundaries were extended by 150″. The footpoint information is predicted using multiple models, provided by Whole Heliosphere and Planetary Interactions (WHPI[3]) during PSP encounters.

2.2. Events Identification

During the selected dates, we cut the region of interest to include the CHs and their adjacent quiet Sun area. The AIA 193 Å images are used to identify ejections events. Ejections in EUV have not been sufficiently statistically studied because of the nature of EUV images of the corona. Besides the fact that the EUV image is complex with dynamic structures, the visibility of the features of interest is very much dependent on the background of said features. To enhance the small transients and to smooth their background of them, we processed the images using a convolution sharpening algorithm proposed by Morgan & Druckmüller (2014).

[3] https://whpi.hao.ucar.edu

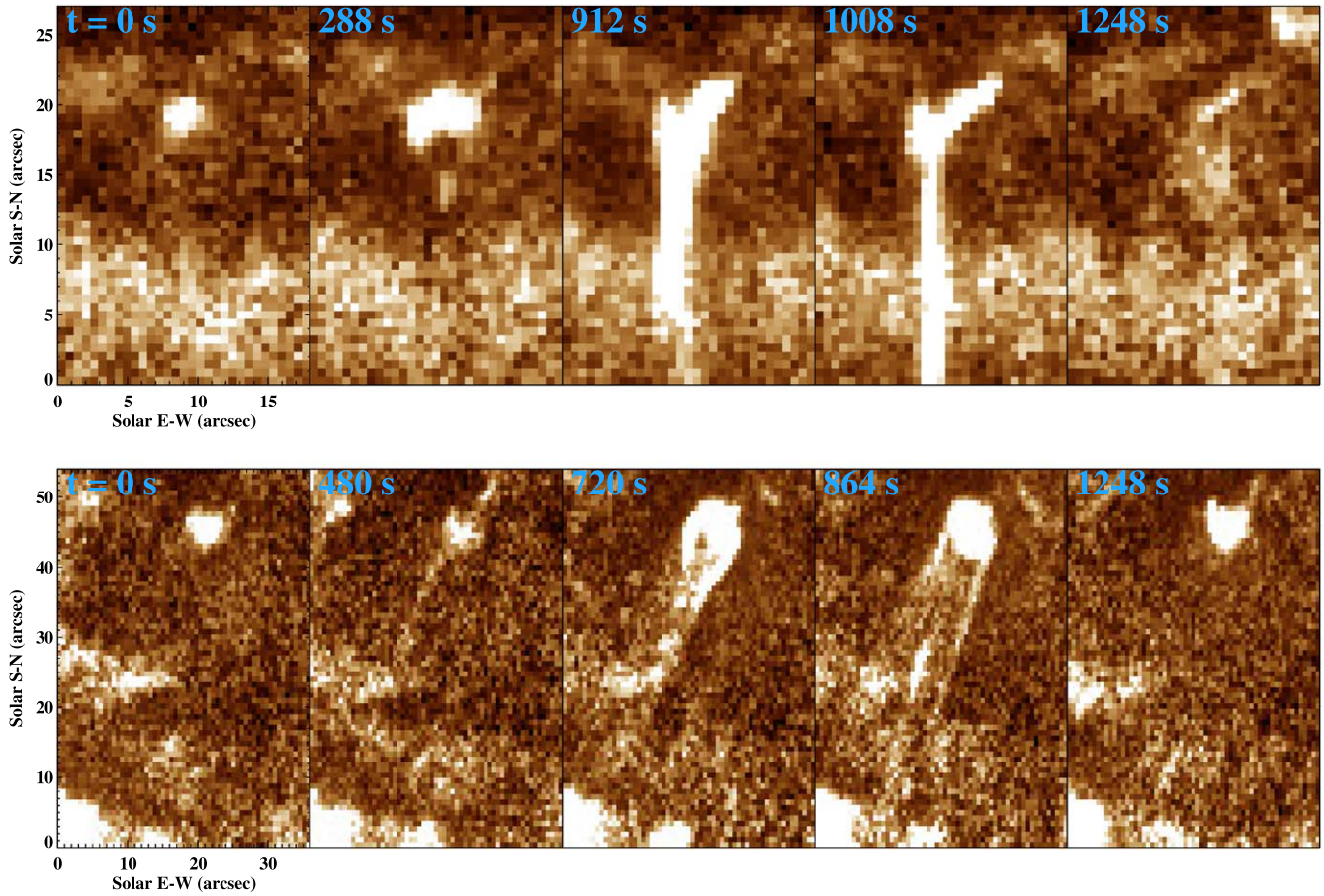

Figure 2. Examples of standard jets (upper panels) and eruptive events (lower panels) identified based on the morphology in AIA 193 Å images. The duration after the onset of the ejection is labeled on each frame. An animation of this figure shows the same examples of the standard jet (left panel) and the eruptive event (right panel). In each frame of the movie, the duration after the onset of the ejections is labeled in the lower left corner (the examples we selected have the same lifetime). The animation runs from $t = 0$ to 1248 s and has a real-time duration of 3 s.

(An animation of this figure is available.)

We used the kernel sizes of 2.5, 5, and 10 pixels (corresponding to 1.″5, 3″, and 6″). Due to the larger convolution kernel, the background area within the image was smoothed. Applying running difference to the convoluted images, the intensity contours are able to denote a large number of transient events. The identified activities are then visually validated. Although we are interested in the ubiquitous transients, we excluded the simple EUV brightening events without visible ejections (jets or breakout motions), assuming that this localized heating in the corona is not able to travel to the heliosphere by solar wind.

Jets are commonly divided into two categories based on their appearances: the standard jets and the blowout jets. This categorization was first based on the soft X-ray images (Moore et al. 2010, 2013). A typical standard jet has an inverted Y shape with a narrow spire and the bright footpoint is stationary to one side of the jet base. The width of the spire and the jet brightening point (JBP) on the base of a blowout jet extends during its lifetime. Using EUV images, Liu et al. (2011) observed a standard jet transform into a blowout jet. Baikie et al. (2022) observed 23 jets using images in soft X-ray as well as in EUV. In their study, the jets and their associated EMF have a clear appearance in 193 Å images. Despite the poor visibility of cool material on 193 Å, the animated movies can show the evolution of events and allow us to categorize the events visually. Figure 2 shows examples of the events we identified and categorized by their morphology in AIA 193 Å images. The movies (available online) show their different morphology and evolution. Although both types of jets are able to be driven by magnetic reconnection and kink instability, the blowout type with minifilament eruption followed by consistent magnetic untwist was considered to be more durable and capable to deliver small transients into the outer corona and solar wind. In Figure 2, the evolution of both types of events is shown—the top panel presents a standard jet, and the bottom panel shows an eruptive jet. The time duration after the onset of the events is labeled on each frame. The standard jet has a stationary narrow spire that forms the Y shape with the brightened base. For the blowout jet, the middle panels present the broadening of the spire. In the movie, a dark structure moving toward the jetting direction is identified as the observational counterpart of EMF. To eliminate the human bias of identification and categorization, the results are validated by different contributors in this study.

3. Results

3.1. Occurrence Rate and Lifetime Distribution

For the days mentioned in Table 1, the jets were identified in the CH regions and adjacent regions. Figure 3 shows the result for the dates in PSP E5. The locations of identified events are overplotted on the 193 Å synoptic map. In Figure 3, the green

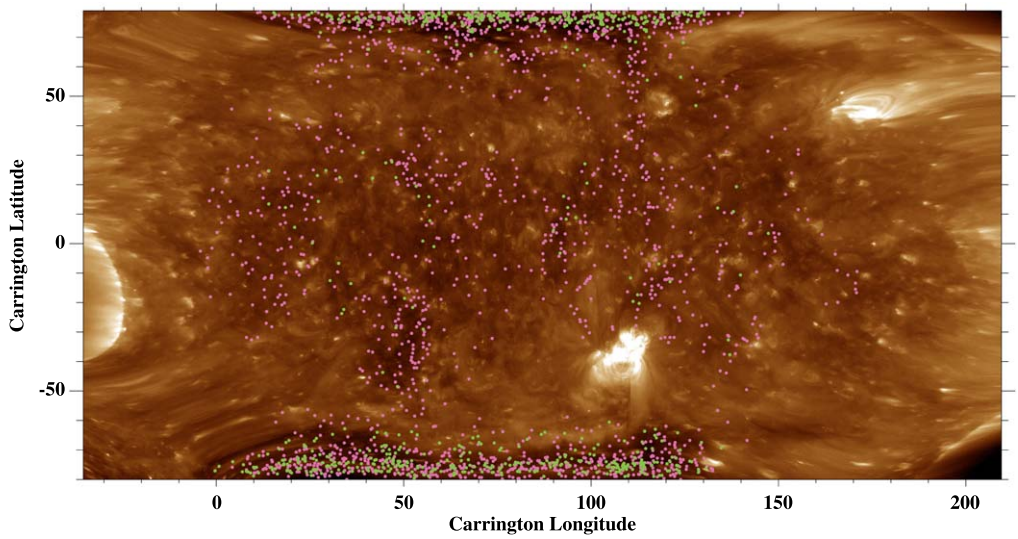

Figure 3. The identified events overplotted on the 193 Å synoptic map. The dates are from 2020 June 9 to 2020 June 13, when the modeled PSP footpoint is in the Earth's side. The green and pink dots represent for locations of identified standard and blowout jets, respectively.

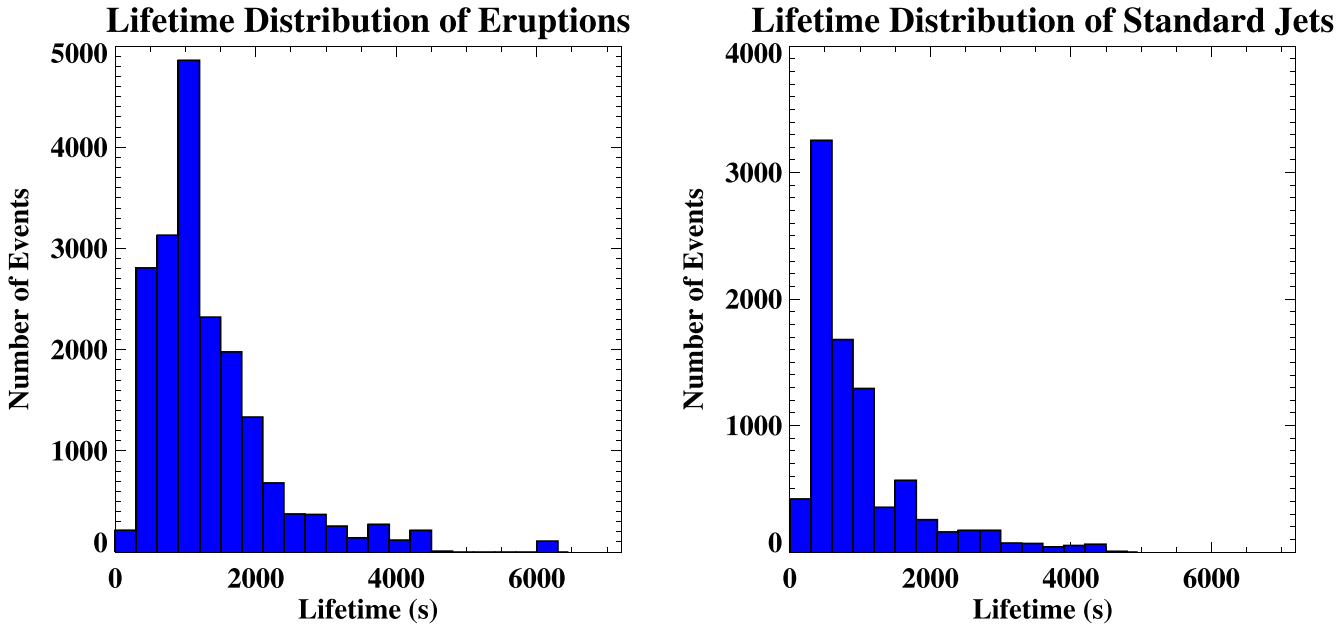

Figure 4. The lifetime distributions of the identified blowout (left panel) and standard (right panel) jets.

and pink dots represent the locations of the standard and blowout jets, respectively. In the 24 days during three encounters, the 8628 standard jets and 19,204 blowout events were identified in the CH regions. Recent studies (e.g., Sterling et al. 2015, 2022) suggest that both blowout and standard jets might result from reconnection induced by an erupting or a partially erupting MF, which suggests that standard jets might also launch Alfvénic pulses into the heliosphere. Therefore, when discussing the influence on the heliospace from such ejections, we consider both standard and blowout jets. Accounting for the area of the CHs we calculated, the occurrence rate is $3.7 \times 10^{-11}\,\mathrm{km}^{-2}\,\mathrm{hr}^{-1}$. Due to the higher spatiotemporal resolution of the observation and the image sharpening process we use, the number of events is over 1 order of magnitude compared to the previous statistical studies. Nevertheless, the occurrence rate is not significantly increased. We will discuss this in the discussion section.

We also collected the lifetime of each event. The lifetime is counted from the start of the eruption of coronal loops (or the first appearance of the jet spire if no loops eruption is observed) until the disappearance of the spire in 193 Å images. For both types of jets, their lifetimes vary from minutes to above 1 hr. Figure 4 shows the histograms of the lifetime of all identified events. The left and right panels are the distributions for blowout and standard jets, respectively. The lifetime of the blowout group is comparatively widely distributed and the typical length is 15–20 minutes. The typical lifetime of standard jets is 5–10 minutes and they are largely distributed in the 5–20 minutes range.

3.2. Jet Base Size Distribution

According to the previous study, the temporal distribution of SB patches can be explained by the PSP footpoint connection to solar supergranule boundaries (Fargette et al. 2021);

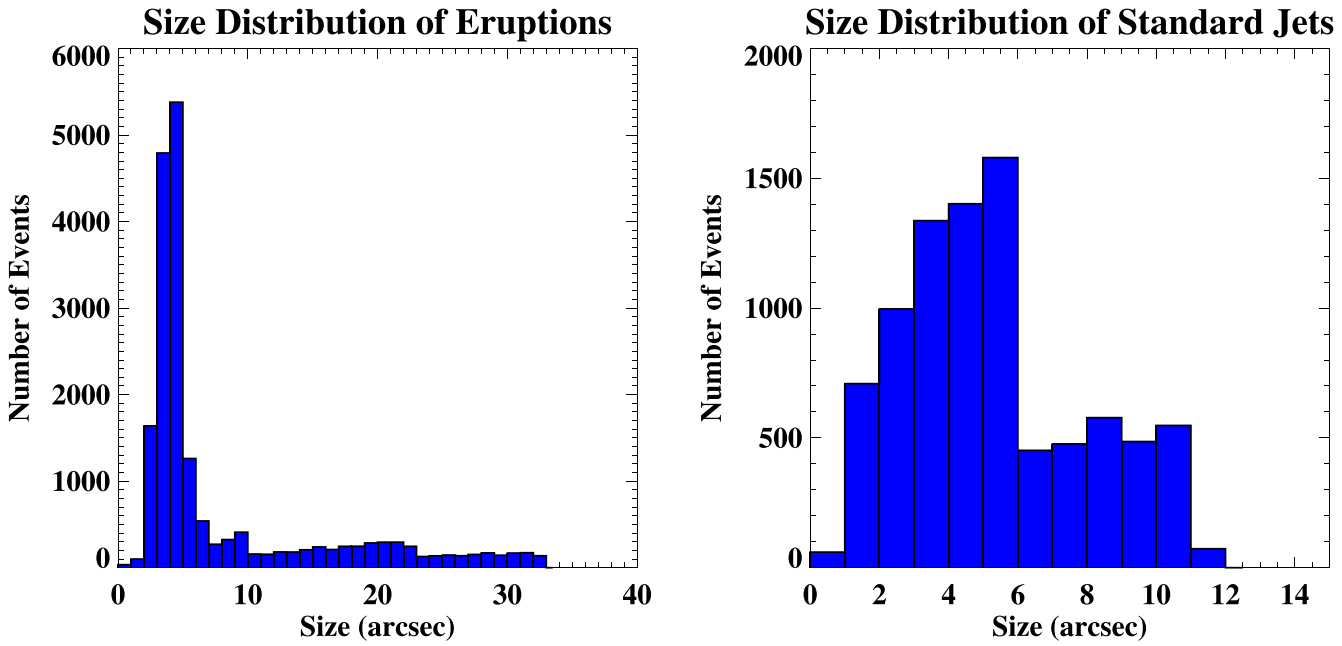

Figure 5. The base size distributions of the identified blowout (left panel) and standard (right panel) jets.

therefore, the modulation in time profile shows a supergranule scale. For the identified ejections, we measure the size of their base. The distribution of their size is plotted in Figure 5. For standard jets, since they typically have an inverted Y shape, the base is brightened and easy to define. In this group, a brightened jet base was contoured by an ellipse and the elongated axis is defined as the size. For the blowout group of jets, the base is comparatively more complicated. Some bases are in large bright loop regions and are inseparable from the background, while some have a lower emission (may because of the temperature or density) or are blocked by the cool filament plasma. For these reasons, we use the maximum width of the broadened eruptive spire as the size of the base. In Figure 5, we plot the jet base size distributions of the two groups of events. For both groups, most of the bases have a size near $\sim 5''$ (3.5 Mm), which is roughly twice the granulation size. Nevertheless, the two groups have obviously different distributions in large-size regimes. The larger standard jets have comparatively smaller bases below $\sim$8 Mm, while the larger blowout group of jets distributes up to $\sim$25 Mm, which is comparable to the size of a supergranule. The sizes of jet bases will be used in the calculation of the expected rate of PSP encountering a CH jet in heliospace.

3.3. Summary and Discussions

We statistically studied the occurrence of coronal jets using AIA 193 Å images during 24 days in PSP's three encounters. Using processed images, we identified 27,832 coronal jets, including 8628 standard jets and 19,204 blowout jets, in the calculated CH regions, and built a database of their time, location, lifetime, and size for further use. Standard jets tend to occur in polar CHs, while blowout jets occur much more frequently in equatorial CHs. However, this difference may be partially due to the projection effect.

Using the EUV images and having identified numerous smaller-scale ejections, it is shown that the solar corona is more active than previously considered. The total occurrence rate of the coronal jets in CH regions by our identification is $3.7 \times 10^{-5}\,\mathrm{hr}^{-1}\,\mathrm{Mm}^{-2}$. The lifetime of standard jets is consistent with the previous study, while the lifetime of blowout jets is double what was previously found (Savcheva et al. 2007; Sako et al. 2013).

In the work of Roberts et al. (2018), the author calculated the frequency that PSP encounters in a CH jet using a simplified approach. They adopted the result from Sako et al. (2013) where the occurrence rate of jets in CH is $S_{\mathrm{chj}\odot} \approx 1 \times 10^{-11}\,\mathrm{km}^{-2}\,\mathrm{hr}^{-1}$ and their average width is $w_{\mathrm{chj}} = 4 \times 10^3$ km. In their approach, a jet must pass within a circle centering on the PSP whose radius is the width (diameter) of a jet base to be detected by PSP. This makes the effective cross section $A_{\mathrm{PSP}} = \pi w_{\mathrm{chj}}^2 \approx 4 \times 10^7\,\mathrm{km}^2$. Based on the assumption that the open field originating from CH would expand and fill the entire heliospace, the expected rate of PSP encountering a CH jet was calculated to be $N_{\mathrm{PSP}} = S_{\mathrm{chj}\odot} \times A_{\mathrm{PSP}} \approx 4 \times 10^{-4}\,\mathrm{hr}^{-1} \approx 1 \times 10^{-2}\,\mathrm{days}^{-1}$.

Using AIA images with higher temporal and spatial resolution, we were able to update the statistical result of ejections in CHs. In our study, the average width and lifetime of identified ejections are the following:

$$w_{\mathrm{ej}} \approx 5 \times 10^3\,\mathrm{km}, \tag{1}$$

$$\tau_{\mathrm{ej}} \approx 20\ \mathrm{minutes}. \tag{2}$$

The average number of ejections in our identified CHs is higher than the number reported in Sako et al. (2013) by over 1 order of magnitude, while the occurrence rate in our calculation is updated to

$$S_{\mathrm{ej}} \approx 3.7 \times 10^{-11}\,\mathrm{km}^{-2}\,\mathrm{hr}^{-1} \tag{3}$$

which is only $\sim$4 times their result. We suspect that they underestimated the CH area in their calculation; hence the occurrence rate was overestimated.

Wang et al. (1996) estimated the energy flux of the solar wind to be over $10^5\,\mathrm{erg\,cm}^{-2}\,\mathrm{s}^{-1}$. Based on the occurrence rate

of the CH ejection, the average energy of these ejections must be 10^{29}–10^{30}erg to deliver enough energy to power the solar wind.

Using the statistical results, we calculate the expected frequency that PSP encounters such ejections near its perihelia. In the work of Roberts et al. (2018), they calculated the expected frequency without considering the lifetime of the CH jets and the traveling of the PSP, which we involve in our algorithm. We adopt some approximations in their work and start with the same method. Since the CH-originated magnetic flux should expand and fill the entire heliospace that PSP travels through, we can map the PSP's path to the CHs on the solar surface. An ejection must exist within a distance less than $w_{\rm ej}$ to PSP to be detected. The effective cross-section area is

$$A'_{\rm PSP\odot} = \pi w_{\rm ej}^2 + 2w_{\rm ej} \cdot v_{\rm PSP\odot} dt \quad (4)$$

where $v_{\rm PSP\odot}$ is the speed of PSP footpoint moving in CHs. During the PSP encounters the projection of PSP on the solar surface moves at a speed that varies from 0 km s^{-1} (during the corotation period) to $\sim$10 km s^{-1} (during the perihelion 8), the speed of the footpoint in CHs becomes 0 to $\sim$26 km s^{-1} since the heliospace is filled with flux from CHs who occupy $\sim$15% of the total solar surface.

On the other hand, for any dt, to exist in the cross section of PSP detection, the starting of an ejection should be ahead of the time for less than the time of the ejection to pass through the sphere of spacecraft, namely $\tau_{\rm ej\_sc}$. Following the suggestion in Sterling & Moore (2020), we consider the propagation of such ejection affecting the outer corona as an Alfvénic twist-wave packet. In the lower solar corona, with the solar wind velocity $v_{\rm sw\odot} = 0$, the packet should travel with the Alfvén velocity $v_{A\odot} \approx 1000$ km s^{-1}. Using data from PSP solar wind electron, alphas, and protons instrument suite (Kasper et al. 2015), we obtain the velocity of background solar wind $v_{\rm sw} \approx 280$ km s^{-1} and the velocity spikes $v_{\rm spike} \approx 100$ km s^{-1} riding over it. Then we get

$$\tau_{\rm ej\_sc} = \frac{v_{A\odot}}{v_{\rm sw} + v_{\rm spike}} \tau_{\rm ej} \approx 53 \text{ minutes}. \quad (5)$$

Therefore, the number of ejections meeting with PSP during dt

$$dN_{\rm PSP} = \int_{-\tau_{\rm ej\_sc}}^{dt} S_{\rm ej} \cdot A'_{\rm PSP\odot} \cdot dt \quad (6)$$

and the expected frequency of PSP encountering the ejections is

$$\begin{aligned} \frac{N_{\rm PSP}}{T} &= \frac{\int_0^T dN_{\rm PSP}}{T} \\ &= \frac{1}{T}\int_0^T \int_{-\tau_{ej\_sc}}^{dt} S_{ej}(\pi w_{ej}^2 + 2w_{ej} v_{\rm PSP\odot} dt) dt \\ &\approx \frac{1}{T}(S_{ej}\pi w_{ej}^2 (T + \tau_{ej\_sc}) + 2S_{ej} w_{ej} v_{\rm PSP\odot} \tau_{ej\_sc} T). \end{aligned} \quad (7)$$

Plugging in the statistical properties of ejections, we obtain the expected frequency, which should vary by the speed of PSP:

$$N'_{\rm PSP\_ej} \approx \begin{cases} 0.12 \text{ day}^{-1} & \text{(corotation)} \\ 0.73 \text{ day}^{-1} & \text{(perihelion)} \end{cases}. \quad (8)$$

It should be noted that $S_{\rm ej}$ in our study should be considered to be the lower limit of the actual occurrence rate of ejections in CHs, in that there are events excluded from our identification due to their lower visibility comparing to the background. The actual $S_{\rm ej}$ should result in a higher frequency that PSP detects a CH ejection.

For such CH ejections, their frequency of encountering PSP is significantly insufficient to be the only source of the SBs, which are detected in situ dozens of times per hour. In Fargette et al. (2021) the authors used wavelet power spectrum (WPS) to analyze the temporal modulation of SBs detection. One of the WPS peaks for SBs patches occurrence was at a period between 13 and 18 hr, corresponding to a repetition pattern of 1.3–1.8 day^{-1}. This rate is higher but comparable to our result, which suggests the ejections as one of the possible activities that generate the SB patches. When such ejections can be driven by interchange reconnection between an open field line rooted in supergranule network lanes and coronal loops, they are able to deliver the released energy to build up patches of SBs into the solar wind. However, according to the discussion in Fargette et al. (2021), the peak at the 13–18 hr period should correspond to the large patches, which is not considered as the typical detected pattern of SBs. As the authors discussed, the realistic period of SB patches is around 2–5 hr during near 5 days around the perihelion, which corresponds to an occurrence rate of $\sim$10 day^{-1}. Therefore, the ejections found in our study should not be sufficient to serve as the only source of the SB patches.

Some ejections with low high-temperature components may be missed by using solely AIA 193 Å images. Although our study extends the identification to ejections with small size which should include some "jetlets," we should not be able to collect all of them. Jetlets were initially used to name the jet-like features brightening on 191 and 193 Å images ejecting from plume base locations, whose base size is smaller (a few arcseconds) and lifetime is shorter (tens of seconds to a few minutes) comparing to typical coronal jets (Raouafi & Stenborg 2014). Panesar et al. (2018) observed such a feature along the edge of network lanes both inside and outside of the plume base region, and named them both jetlets. They found that the jetlets have many similarities with larger coronal jets, other than the scale. Their average base width is $\sim$4000 km and lifetime is $\sim$3 minutes. Using EUV 172 Å images from High-resolution Coronal Imager 2.1 (Hi-C 2.1), Panesar et al. (2019) identified some finer (spire width down to $\sim$600 km) events, and some of them do not even have a brightened base. Considering the cadence and image scale of the data used in our study, the jetlets with lifetime shorter than 2.5 minutes or base width less than 1.″2 may not be detected in our study. Moreover, the events observed in Panesar et al. (2018, 2019) also resolved in the Interface Region Imaging Spectrograph (IRIS; Pontieu et al. 2014). The studies about jetlets extended the boundary of coronal jets, and the jetlets' locating at the edge of network lanes and their occurrence rate make them comparable to type II chromospheric spicules (Yamauchi et al. 2002). Raouafi et al. (2023) used high-resolution data from Goode Solar Telescope (GST; Cao et al. 2010) to observe a 70″ × 70″ field of view in a CH boundary region in near 1.5 hr and identified 61 Hα spicules rooted on network lanes, among which seven had EUV detectable jetlets. Accordingly, the jetlets occurrence rate, $S_{\rm jl} \approx 1.8 \times 10^{-9}$ km^{-2}hr^{-1}, is $\sim$50 times to the occurrence rate of the ejections in our study. Due to the limited database, this

result may not be global. Nevertheless, it is still reasonable to suggest that such events with tens of times higher occurrence rates should better support the formation of SB patches. Furthermore, Lee et al. (2022) observed chromospheric spicules using GST Hα images and suggested that their number along a network is consistent with SBs in patches.

On the other hand, the SMFRs appear to be much closer in count rate comparing to the CH ejections. Zhao et al. (2020) and Chen et al. (2020) identified SMFR using PSP data with wavelet-based and Grad–Shafranov-based (GS-based) analysis, respectively. Zhao et al. (2020) found 40 SMFR in 31 days (2018 October 22 to November 21) and Chen et al. (2020) found 44 in 27 days during PSP E1 and E2 (2018 October 31 to November 14 and 2019 March 7 to April 18). Chen et al. (2021) applied the GS-based analysis to E1–E5 and identified 243 events in 116 days. They discussed the E5 when PSP may have gone through the heliospheric current sheet, which leads to a significantly larger amount of SMFR. Accounting only E1–E4, the SMFR occurrence rate ($\sim$1.3 day^{-1}), which is still twice of but comparable to the frequency of ejection in our study. It should be noted that they identified two types of flux ropes in the study, and what we call SMFR is named a flux rope in their paper, referring to the static flux rope, which is different from the other type of flux ropes with significant field-aligned flow. Moreover, the duration of SMFRs also matches our result (Please refer to Chen et al. 2020, Table 3). Strictly speaking, $N'_{\mathrm{PSP\_ej}}$, the frequency that PSP is expected to detect the CH ejections identified in our study is slightly lower than SMFR. Nevertheless, we are suggesting the ejections as possible candidate of such solar wind transients considering the fact that the occurrence rate of identified ejections used in calculation, $S_{\mathrm{chj}_\odot}$, is the lower limit of the actual occurrence rate of coronal ejections. The visibility of such small ejections is highly affected by the brightness of background and the viewing perspective that makes the spire short visually. This includes the events whose sizes and lifetimes fall in our identification region, but are neglected.

As a summary to our statistical study, the occurrence frequency of the coronal ejections detected in the CH area using EUV (AIA 193) images are of a rate of 0.12–0.73 day^{-1}. This rate is far less than the rate of PSP-detected SBs (several hundred per day) or even the SB patches (several to 10 day^{-1}). However, this investigation determined that the EUV-ejection rate is comparable to the rate of observed heliospheric SMFRs ($\sim$1.3 day^{-1}). Most jetlets are smaller, short-lived events, which are not detected by this study. They might be able to fill the gap for the much more frequent SB patches.

This work was supported by NASA grants 80NSSC19K0257 and 80NSSC20K1282, and NSF grants AGS 2114201 and AGS-2229064.

ORCID iDs

Nengyi Huang https://orcid.org/0000-0001-9049-0653
Haimin Wang https://orcid.org/0000-0002-5233-565X

References

Agapitov, O. V., Drake, J. F., Swisdak, M., et al. 2022, ApJ, 925, 213
Baikie, T. K., Sterling, A. C., Moore, R. L., et al. 2022, ApJ, 927, 79
Bale, S. D., Badman, S. T., Bonnell, J. W., et al. 2019, Natur, 576, 237
Balogh, A., Forsyth, R. J., Lucek, E. A., Horbury, T. S., & Smith, E. J. 1999, GeoRL, 26, 631
Bourouaine, S., Perez, J. C., Klein, K. G., et al. 2020, ApJL, 904, L30
Burlaga, L. F., Klein, L., Sheeley, N. R., Jr., et al. 1982, GeoRL, 9, 1317
Cao, W., Gorceix, N., Coulter, R., et al. 2010, AN, 331, 636
Chen, J. 2017, PhPl, 24, 090501
Chen, Y., & Hu, Q. 2022, ApJ, 924, 43
Chen, Y., Hu, Q., & le Roux, J. A. 2019, ApJ, 881, 58
Chen, Y., Hu, Q., Zhao, L., et al. 2020, ApJ, 903, 76
Chen, Y., Hu, Q., Zhao, L., Kasper, J. C., & Huang, J. 2021, ApJ, 914, 108
Cheng, X., Guo, Y., & Ding, M. 2017, ScChD, 60, 1383
de Wit, T. D., Krasnoselskikh, V. V., Bale, S. D., et al. 2020, ApJS, 246, 39
Drake, J. F., Agapitov, O., Swisdak, M., et al. 2021, A&A, 650, A2
Fargette, N., Lavraud, B., Rouillard, A. P., et al. 2021, ApJ, 919, 96
Fargette, N., Lavraud, B., Rouillard, A. P., et al. 2022, A&A, 663, A109
Feng, H. Q., Wu, D. J., Lin, C. C., et al. 2008, JGRA, 113, A12105
Fisk, L. A., & Kasper, J. C. 2020, ApJL, 894, L4
Forsyth, R. J., Balogh, A., Horbury, T. S., et al. 1996, A&A, 316, 287
Fox, N. J., Velli, M. C., Bale, S. D., et al. 2015, SSRv, 204, 7
Garton, T. M., Gallagher, P. T., & Murray, S. A. 2018, JSWSC, 8, A02
Hou, Z., Tian, H., Berghmans, D., et al. 2021, ApJL, 918, L20
Kasper, J. C., Abiad, R., Austin, G., et al. 2015, SSRv, 204, 131
Kasper, J. C., Bale, S. D., Belcher, J. W., et al. 2019, Natur, 576, 228
Kim, Y.-H., Moon, Y.-J., Park, Y.-D., et al. 2007, PASJ, 59, S763
Krieger, A. S., Timothy, A. F., & Roelof, E. C. 1973, SoPh, 29, 505
Laker, R., Horbury, T. S., Bale, S. D., et al. 2021, A&A, 650, A1
Lee, J., Yurchyshyn, V., Wang, H., et al. 2022, ApJL, 935, L27
Lemen, J. R., Title, A. M., Akin, D. J., et al. 2012, SoPh, 275, 17
Liu, C., Deng, N., Liu, R., et al. 2011, ApJ, 735, L18
Mandal, S., Chitta, L. P., Peter, H., et al. 2022, A&A, 664, A28
Moldwin, M. B., Ford, S., Lepping, R., Slavin, J., & Szabo, A. 2000, GeoRL, 27, 57
Moore, R. L., Cirtain, J. W., Sterling, A. C., & Falconer, D. A. 2010, ApJ, 720, 757
Moore, R. L., Sterling, A. C., & Falconer, D. A. 2015, ApJ, 806, 11
Moore, R. L., Sterling, A. C., Falconer, D. A., & Robe, D. 2013, ApJ, 769, 134
Morgan, H., & Druckmüller, M. 2014, SoPh, 289, 2945
Myers, C. E., Yamada, M., Ji, H., et al. 2017, PPCF, 59, 014048
Panesar, N. K., Sterling, A. C., Moore, R. L., et al. 2018, ApJ, 868, L27
Panesar, N. K., Sterling, A. C., Moore, R. L., et al. 2019, ApJ, 887, L8
Pecora, F., Matthaeus, W. H., Primavera, L., et al. 2022, ApJL, 929, L10
Pesnell, W. D., Thompson, B. J., & Chamberlin, P. C. 2012, SoPh, 275, 3
Pontieu, B. D., Title, A. M., Lemen, J. R., et al. 2014, SoPh, 289, 2733
Raouafi, N., Stenborg, G., Seaton, D., et al. 2023, ApJ, 945, 28
Raouafi, N. E., Patsourakos, S., Pariat, E., et al. 2016, SSRv, 201, 1
Raouafi, N.-E., & Stenborg, G. 2014, ApJ, 787, 118
Roberts, M. A., Uritsky, V. M., DeVore, C. R., & Karpen, J. T. 2018, ApJ, 866, 14
Sako, N., Shimojo, M., Watanabe, T., & Sekii, T. 2013, ApJ, 775, 22
Savcheva, A., Cirtain, J., DeLuca, E. E., et al. 2007, PASJ, 59, S771
Schwadron, N. A., & McComas, D. J. 2021, ApJ, 909, 95
Shibata, K., Ishido, Y., Acton, L. W., et al. 1992, PASJ, 44, L173
Squire, J., Chandran, B. D. G., & Meyrand, R. 2020, ApJL, 891, L2
Sterling, A. C., & Moore, R. L. 2020, ApJL, 896, L18
Sterling, A. C., Moore, R. L., Falconer, D. A., et al. 2016, ApJ, 821, 100
Sterling, A. C., Moore, R. L., Falconer, D. A., & Adams, M. 2015, Natur, 523, 437
Sterling, A. C., Moore, R. L., & Panesar, N. K. 2022, ApJ, 927, 127
Telloni, D., Zank, G. P., Stangalini, M., et al. 2022, ApJL, 936, L25
Tenerani, A., Velli, M., Matteini, L., et al. 2020, ApJS, 246, 32
Wang, J., Li, W., Denker, C., et al. 2000, ApJ, 530, 1071
Wang, Y.-M., Hawley, S. H., & Sheeley, N. R. 1996, Sci, 271, 464
Wang, Y.-M. N. R., Sheeley, J., Socker, D. G., et al. 1998, ApJ, 508, 899
Wyper, P. F., Antiochos, S. K., & DeVore, C. R. 2017, Natur, 544, 452
Wyper, P. F., DeVore, C. R., & Antiochos, S. K. 2018, ApJ, 852, 98
Yamauchi, Y. 2004, JGRA, 109, A03104
Yamauchi, Y., Suess, S. T., & Sakurai, T. 2002, GeoRL, 29, 21
Yang, S., & Zhang, J. 2018, ApJL, 860, L25
Yokoyama, T., & Shibata, K. 1995, Natur, 375, 42
Zhao, L.-L., Zank, G. P., Adhikari, L., et al. 2020, ApJS, 246, 26
Zheng, J., & Hu, Q. 2018, ApJL, 852, L23
Zirker, J. B. 1977, RvGeo, 15, 257